Original Research

# The Fat-glandular Interface and Breast Tumor Locations: Appearances on Ultrasound Tomography Are Supported by Quantitative Peritumoral Analyses

**Peter J. Littrup, MD,**[1,2,3,*] **Nebojsa Duric, PhD,**[1,2,3] **Mark Sak, PhD**[3]
**Cuiping Li, PhD,**[3] **Olivier Roy, PhD,**[3] **Rachel F. Brem, MD FACR FSBI,**[4]
**Mary Yamashita, MD**[5]

[1]Departments of Radiology and Oncology, Karmanos Cancer Institute, Detroit, MI, USA; [2]Department of Oncology, Wayne State University, Detroit, Novi, MI, USA; [3]Delphinus Medical Technologies, Inc., Novi, MI, USA; [4]The George Washington Cancer Center, George Washington University, Washington, DC, USA; [5]University of Southern California; Norris Cancer Center and Hospital, Los Angeles, CA, USA

*Address correspondence to P.J.L. (e-mail: pjlittrup@gmail.com)

## Abstract

**Objective:** To analyze the preferred tissue locations of common breast masses in relation to anatomic quadrants and the fat-glandular interface (FGI) using ultrasound tomography (UST).

**Methods:** Ultrasound tomography scanning was performed in 206 consecutive women with 298 mammographically and/or sonographically visible, benign and malignant breast masses following written informed consent to participate in an 8-site multicenter, Institutional Review Board-approved cohort study. Mass locations were categorized by their anatomic breast quadrant and the FGI, which was defined by UST as the high-contrast circumferential junction of fat and fibroglandular tissue on coronal sound speed imaging. Quantitative UST mass comparisons were done for each tumor and peritumoral region using mean sound speed and percentage of fibroglandular tissue. Chi-squared and analysis of variance tests were used to assess differences.

**Results:** Cancers were noted at the FGI in 95% (74/78) compared to 51% (98/194) of fibroadenomas and cysts combined ($P < 0.001$). No intra-quadrant differences between cancer and benign masses were noted for tumor location by anatomic quadrants ($P = 0.66$). Quantitative peritumoral sound speed properties showed that cancers were surrounded by lower mean sound speeds (1477 m/s) and percent fibroglandular tissue (47%), compared to fibroadenomas (1496 m/s; 65.3%) and cysts (1518 m/s; 84%) ($P < 0.001$; $P < 0.001$, respectively).

**Conclusion:** Breast cancers form adjacent to fat and UST localized the vast majority to the FGI, while cysts were most often completely surrounded by dense tissue. These observations were supported by quantitative peritumoral analyses of sound speed values for fat and fibroglandular tissue.

**Key words:** ultrasound tomography; tumor location; breast cancer; fibroadenoma; cyst; fat-glandular interface.

**Key Messages**

- The majority of breast cancers (95%) are located at the circumferential fat-glandular interface (FGI), a high-contrast structure by sound speed (SS) in the coronal plane.
- Tissue locations for cysts also suggest they are more likely (64%) to be surrounded by fibroglandular tissue, while fibroadenomas are intermediate in location at the FGI (63%) and surrounded by fibroglandular tissue (35%).
- Location of masses relative to the fat-glandular interface may be useful to incorporate in computer-aided US diagnostics for screening in women with dense breasts.

## Introduction

Breast cancer locations can be described relative to their imaging appearance and histopathologic origins. Mammographically, greater cancer incidence within the upper outer quadrants (1,2) has been ascribed to greater parenchymal content or epithelial distribution (2,3), which can obscure cancer detection in women with dense breasts. Breast MRI has used percent fibroglandular volume as a surrogate for localized breast density, but only 20% of cancer locations corresponded to the quadrant with the highest density (ie, percent fibroglandular volume) (4). The fat-glandular interface (FGI) has also been noted on MRI as the dominant location for up to 94%–99% of clinical breast cancers, but they did not address cysts or evaluate the coronal imaging plane (5,6). Automated breast ultrasound (ABUS) is used for screening women with dense breasts (7,8), correlates well with MRI fibroglandular volume (9), and its reconstructed coronal view improves both reading efficiency (10) and mass discrimination (11).

Unlike supine ABUS examinations requiring 2–5 scan acquisitions per breast depending on breast size (7), ultrasound tomography (UST) images the prone breast in a single coronal acquisition. UST technical progress has accelerated over the last 40 years (12–21), with much greater computing capacity allowing clinically relevant scan times, image processing, and quantitative computer-assisted criteria. SoftVue prototype (Delphinus Medical Technologies Inc, Novi, MI) with a ring array UST transducer (22) can scan the whole breast and detect underlying masses by combining coronal acquisitions of reflection, sound speed (SS), and attenuation data (13–19, 21–23) [Table 1, Figure 1]. SS imaging shows high contrast between fat and fibroglandular tissues, especially using recent algorithm improvements (17). Whole breast SS measurements have shown close correlation with mammographic breast density (15,16,18,19,21,22), and MRI fibroglandular volume (19) and may be a stronger breast cancer risk factor than mammographic density (21). Reduction in tumor SS following neoadjuvant chemotherapy has also been used in conjunction with tumor size to prognosticate complete tumor response (23).

**Table 1.** Clinical SoftVue (Delphinus) Operating Parameters

| UST operating parameters | Details |
| --- | --- |
| Number of transducer elements | 2048 |
| Maximum breast diameter | 22 cm |
| Anatomic coverage—visualized | Pectoralis muscle to nipple |
| Operating frequency | 3 MHz |
| Imaging resolution (volume) | $0.7 \times 0.7 \times 2.5$ mm |
| Data acquisition time per breast | ~2 min. |
| Reconstruction time per slice | 4 sec. |
| Patient throughput (projected) | 4/hr. |
| Radiologists review time (~complexity) | 2–4 min. |
| #Slices per stack (~breast size) | ~30–60 |
| *Image stacks-type:* | Reflection |
| | Sound Speed |
| *(SS-corrected Reflection)* | Wafer |
| *(SS + ATT overlaid on Reflection)* | Stiffness Fusion |

Abbreviations: ATT, attenuation; MHz, megahertz; SS, sound speed; UST, US tomography.

Breast cancer initiation and growth have strong associations with peritumoral fat cells, or adipocytes, and their fat-secreted hormones, adipokines, that mediate blood pressure, reproductive function, appetite, glucose homeostasis, angiogenesis, immune function, and cancer growth (24–28). Adipokines, such as leptin, have been implicated in the initiation of breast cancer via aromatase expression when the balance tips toward an excessive proinflammatory state (26–28). Tumor growth of cancer cell lines become markedly accelerated in the presence of cancer-associated adipocytes and adipocyte-derived fibroblasts that contribute to breast cancer progression. These complex peritumoral stromal processes may correlate with hyaluronan deposition and peritumoral apparent diffusion coefficient values by breast MRI (29,30), as well as a stiff peritumoral rim by shear wave elastography (31,32). The FGI thus describes the fibroglandular boundaries with the subcutaneous adipose layer, which may represent the largest endocrine source for breast cancer origin and growth (26).

We hypothesize that cancers will also be preferentially found by UST at the FGI, which is well seen by sound speed imaging in the native coronal imaging plane, and that quantitative tissue properties can objectively differentiate cancers from benign masses, including cysts.

## Materials and Methods

### Subjects

For this study, data were used from the clinical diagnostic arm of an 8-site multicenter Institutional Review Board approved, Health Insurance Portability and Accountability Act compliant study of SoftVue UST for dense breast screening (clinicaltrials.gov—NCT #02977247). All participants gave written informed consent for study participation for this observational descriptive cohort study.
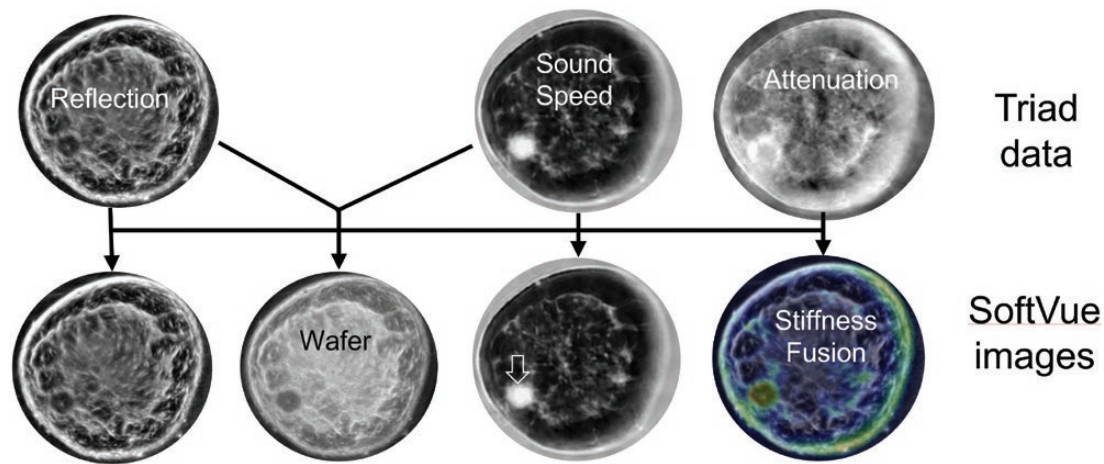
**Figure 1.** Each breast is scanned in the coronal plane by a ring array transducer (22) acquiring the data triad of reflection, sound speed, and attenuation (top row). Four SoftVue (Delphinus) image stacks (bottom row) then consist of reflection, wafer (waveform enhanced reflection), sound speed, and stiffness fusion. Arrows show composite imaging of sound speed-corrected reflection for wafer and the combination of sound speed and attenuation overlaid upon reflection for stiffness fusion. The irregular 1.2 cm high sound speed mass that is an invasive cancer noted at the 8 o'clock position (open arrow) thereby impacts the wafer image, making the cancer better seen than on reflection.

Women of all breast densities were eligible to receive additional UST imaging as part of their clinical visit for evaluation of a palpable or mammographic abnormality. The main inclusion criterion was their willingness to participate with a SoftVue scan during their clinical visit. Exclusion criteria included age <18 years, body weight >350 pounds (ie, SoftVue scanning table projected limit), inability to provide informed consent, inability to lie prone on the UST table, and any open sores or wounds on the breast precluding immersion into the UST water bath for their own safety (ie, sanitized water is exchanged by the system between each patient). No comparable data overlap is noted with any prior or current publications.

## Image Acquisition and Analyses

All masses were included between UST scan dates 4/2017-10/2018 for this consecutive data set, using the same version of the SoftVue unit and associated reconstruction algorithms across all centers of the trial. The SoftVue unit displays image acquisition in the coronal plane (Figure 1) and Table 1 gives clinically relevant performance parameters (13–19,21,22). To avoid associations with mammographic density, dense breast parenchyma was referred to as fibroglandular tissue and segmented from fat by SS (15,18,19,21,22). All identified masses on UST were biopsy-confirmed by subsequent or prior histology, unless considered as a characteristic cyst by ultrasound criteria. All complicated cysts underwent aspiration with cytologic confirmation. Some women had more than one mass in each or both breasts.

### Qualitative Tumor Locations
Mass locations in relation to their anatomic quadrants and FGI were recorded by a central reviewing radiologist (PJL)

not affiliated with any of the participating trial sites, with extensive UST experience and 23 years of experience in breast imaging. Masses were categorized according to standard quadrant positions (ie, upper outer, upper inner, lower outer, lower inner) based on distance from the nipple and clock position of the mass on coronal UST, comparing with available clinical imaging (ie, mammography, handheld US and/or breast MRI) for concordance. If a mass location was along a border of 2 adjacent quadrants, it was considered within the quadrant containing the greatest bulk of the tumor on UST.

The boundaries of the FGI were defined on coronal SS images as the high contrast interface between bright fibroglandular tissue and the circumferential darker subcutaneous fat (5,6) (Figure 2). UST tissue locations were visually sorted into 3 groups: (1) completely surrounded by higher SS (m/sec) fibroglandular tissue, (2) completely surrounded by lower SS fat, or (3) partially surrounded by both (ie, at the FGI) (Figure 2), rather than using previously reported subjective percentages of mass extension into fat and/or fibroglandular tissue (6), or simply being noted at the FGI (7). A mass could thereby be considered as being at the FGI if, at one extreme, it was surrounded by fibroglandular tissue but abutted a small margin of fat, or conversely if it was surrounded by fat yet abutted adjacent fibroglandular tissue.

### Quantitative Tumor Locations
Mass boundaries were hand-traced by the reviewing radiologist to generate quantitative regions of interest (ROIs) using MIM viewing software (MIM Software Inc, Cleveland, OH). Mass margins were traced on their best visualized appearance on a single SS and/or reflection image to generate ROI surface areas (Figure 3). Once tumor margins were traced, a peritumoral ROI was
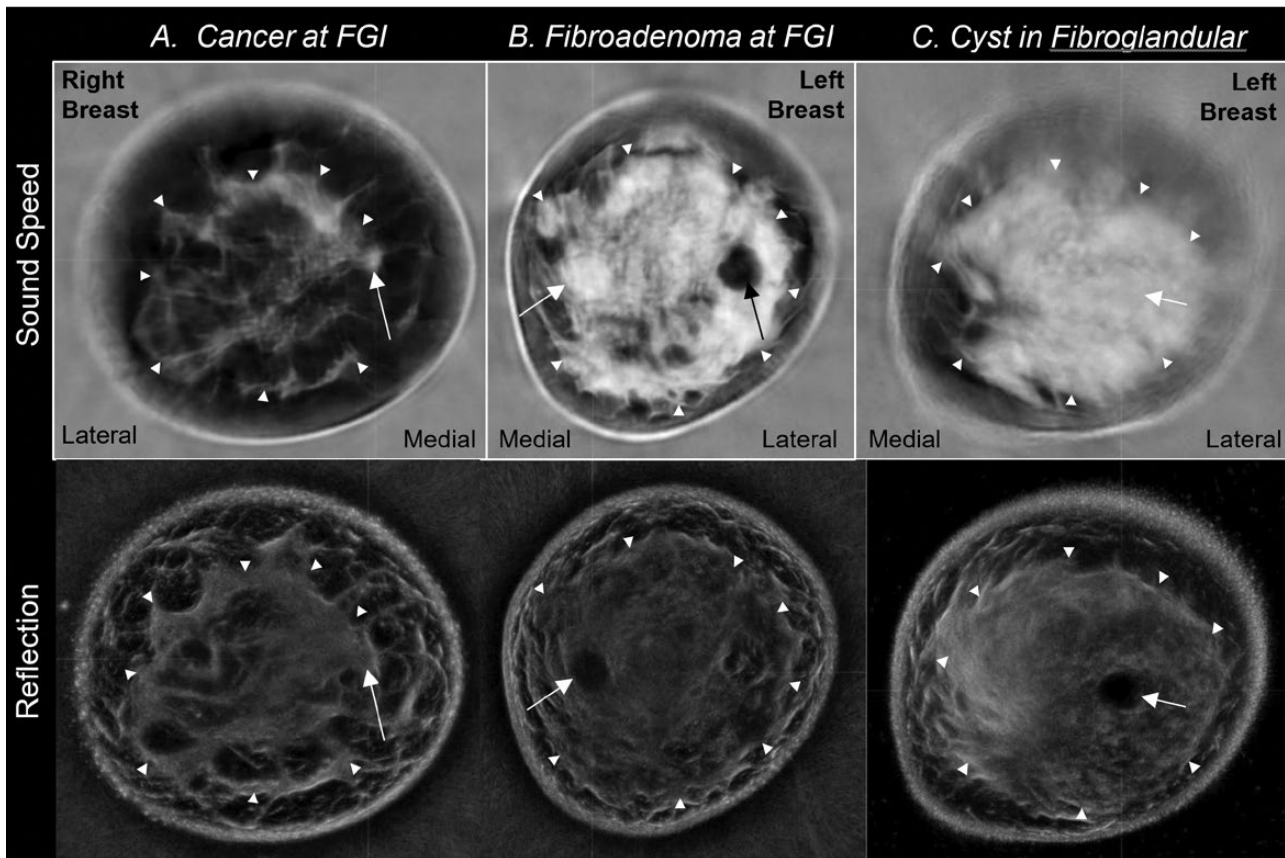
**Figure 2.** Qualitative locations of a cancer, fibroadenoma, and cyst as seen on ultrasound tomography sound speed (SS-top row) and reflection (bottom row). **A**: 45-year-old woman with heterogeneously dense breast parenchyma and a mildly spiculated 0.7 cm mass that is an invasive cancer (arrow) in the right upper inner quadrant at the fat-glandular interface (FGI) (arrowheads). It is best seen on SS and is ill-defined on reflection, a common finding for small cancers. **B**: 52-year-old woman with extremely dense breast parenchyma and a 1.6 cm fibroadenoma (white arrow) in the left lower inner quadrant at the FGI (arrowheads). Note that the mass is abutting fat on a small margin, which is more conspicuous on reflection. A fat lobule surrounded by parenchyma creates a pseudomass (black arrow). **C**: 40-year-old woman with extremely dense breast parenchyma and a 1.5 cm simple cyst (arrow) located within the fibroglandular tissue of the left breast, best seen on reflection and obscured by the diffuse white parenchyma on SS. The SS image shows refraction artifacts blurring the upper and lateral skin margins, compatible with its posterior level as the breast extends toward the axilla, seen only as a thicker skin line on reflection.

computer-generated by dilating the tumor margins by 20% of the average tumor diameter, comparable to a symmetric peritumoral "band" (30). The 20% diameter expansion was arbitrarily chosen as a representative compromise, rather than using the complexity of sequential concentric rings (29,30) at this time, which allowed the peritumoral band to remain proportionate for every tumor.

Mean SS values for each tumor and its peritumoral ROI allowed calculations of their differences and ratios between mass types. The tumoral and peritumoral ROIs were further segmented into two regions by SS, corresponding to fibroglandular and fatty tissues using k-means clustering (15,16,18,19,21,22). This allowed for similar comparisons of percent fibroglandular tissue between each ROI and mass type. The amount of fat and/or fibroglandular tissue surrounding masses could thus be quantified and compared between masses.

## Statistical Analyses

The study used only descriptive statistics and was not powered to define a specific hypothesis. Comparisons of mean values between the mass types were performed using analysis of variance (ANOVA) analyses. Chi-squared tests were used to assess frequency differences with significance declared at $P < 0.05$.

## Results

A total of 206 women (239 breasts) were included in this study. The average age for study participants was 48.9 years (standard deviation 11.6 years, range 18–82 years). A total of 298 benign and malignant breast masses were noted within 239 breasts (Table 2). Average tumor diameter was larger for cancers as compared to fibroadenomas and cysts (1.3 cm, 1.1 cm, and 1.0 cm, respectively, $P = 0.007$
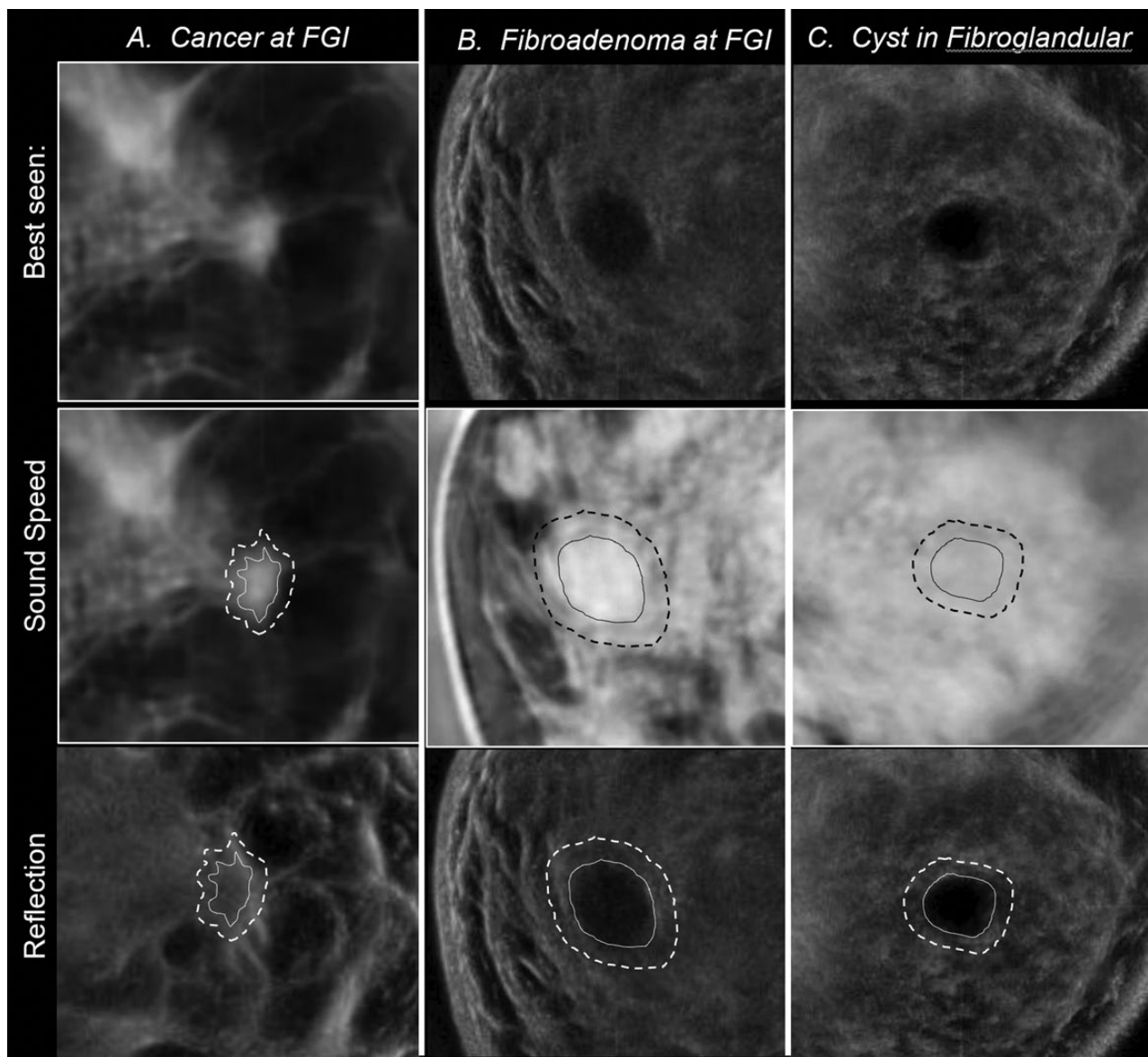
**Figure 3.** Graphic representations of ROI process for obtaining quantitative evaluations of the magnified masses noted from Figure 2. The masses were best seen (top row) on sound speed (SS) for the small cancer and reflection for the fibroadenoma and cyst. The tumor margins (solid line) and peritumoral (dashed line) regions were then traced on both SS (middle row) and reflection (bottom row) images. Pixels within the tumor and peritumoral regions were then objectively segmented into fat or fibroglandular sound speed values noted in Table 4. Abbreviation: ROI, region of interest.

ANOVA), with 81% (241/298) of masses <1.5 cm (Table 2). Hormonal receptors and other tumor markers were not available within the trial database. The distribution of mammographic densities for this clinical data set were 8.7% (18/206) scattered, 64.6% (133/206) heterogeneously and 26.7% (55/206) extremely dense.

**Qualitative Tumor Locations**
The four-quadrant anatomic distribution (Table 3) showed significantly greater cancer occurrence of 43.6% (34/78) within the upper outer quadrant compared to other quadrants (chi-squared, $P = 0.001$). Similarly, 37.1% (39/105) of

fibroadenomas and 42.9% (39/91) of cysts were also more commonly seen in the upper outer quadrant (chi squared $P = 0.003$ and $P < 0.001$, respectively), such that no significant trend was noted separating individual tumor types in the upper outer quadrant ($P = 0.648$), as well as when comparing cancer with the group of all benign masses ($P = 0.688$). All tumors were least commonly located in the lower inner quadrant.

Cancers were visually classified at the FGI in 94.9% (74/78) of cases, which was highly significant compared to being completely surrounded by fat or fibroglandular tissue (chi-squared, $P < 0.001$) (Table 3). For benign masses, their individual values of 62.9% (66/105) of

fibroadenomas and 36.3% (33/91) of cysts as well as when grouped into all benign masses of 54.5% (120/220) were significantly more commonly located at the FGI (Table 3) (*P* < 0.001 and *P* < 0.001 respectively). Moreover, 63.7% (58/91) of cysts and 25.0% (37/105) of fibroadenomas were fully surrounded by dense tissue, which was much more than cancers (0/78, 0%) with those opposing trends best visualized in Figure 4. Few cancers (4/78, 5.1%), fibroadenomas (2/105, 1.9%), or cysts (0/91, 0%) were completely surrounded by fat. Overall, cancers had a different distribution relative to the FGI location compared to benign histologies (*P* < 0.001). Using cancer location for possible test performance criteria (Table 3) showed that the FGI had 95% sensitivity (74/78) and 38% positive predictive value (74/120), which were both higher than the upper outer quadrant having 44% sensitivity (34/78) and 29% PPV (34/85). For any particular anatomical location, there was no predominant FGI location (*P* = 0.19).

### Quantitative Tumor Locations

Mean quantitative SS and percent fibroglandular tissue were grouped according to mass type for the tumoral and peritumoral regions in Table 4. The peritumoral region of cancers had the lowest mean SS and percent fibroglandular tissue (1477 m/s and 47.1%), whereas cysts had the highest values (1518 m/s and 84.0%) and fibroadenomas were intermediate (1496 m/s and 65.3%). These quantitative results support the qualitative location results and were indicative of cancers at the FGI being surrounded by both fatty and dense tissue, while cysts were more frequently surrounded by dense tissue. Considering all masses, those located at the FGI had lower mean peritumoral SS and percent fibroglandular tissue than masses located in dense tissue (1484 m/s versus 1524 m/s, *P* < 0.001; and 53.3% versus 90.7%, *P* < 0.001, respectively).

Boxplots of the peritumoral SS and percent fibroglandular tissue grouped by mass type are seen in Figure 5. Although there is overlap between cancers and fibroadenomas, in particular, the median peritumoral percent fibroglandular tissue for cysts and cancers are 98.5% and 44.7%, respectively. The majority of the cysts are thus almost entirely surrounded by dense tissue, while cancers are surrounded more by fat.

## Discussion

The results of our study show that UST localizes 95% (74/78) of cancers to the FGI, which is seen as a high contrast interface between fat and fibroglandular tissue on coronal sound speed imaging. Conversely, only 55% (120/220) of all benign masses were noted at the FGI (*P* < 0.001), whereby only cysts were predominantly surrounded by fibroglandular tissue (64%) and a minority of fibroadenomas (35%). All masses were more common in the upper outer quadrant, such that anatomic location

**Table 2.** Mass Type and Size Distributions, Including Subtypes of Cancer and Other Benign Categories as Noted. The Smaller (ie, <1.5 cm) Other Benign Commonly Showed Underlying Fibrosis Noted from Biopsy Reports

| Mass histology | Count (*N*) | <1.5 cm | >1.5 cm |
|---|---|---|---|
| Cancer—all | 78 | 52 | 26 |
| IDC | 57 | 37 | 20 |
| DCIS alone | 6 | 5 | 1 |
| IDC + DCIS | 2 | 2 | 0 |
| ILC | 10 | 5 | 5 |
| Other | 3 | 3 | 0 |
| Benign—all | 220 | 189 | 31 |
| Fibroadenoma | 105 | 88 | 17 |
| Cyst | 91 | 80 | 11 |
| Other benign | 24 | 21 | 3 |
| Totals | 298 | 241 | 57 |

Other cancers include 1 mammary, 1 mucinous, and 1 papillary carcinoma. Other benign masses include 21 containing fibrosis, two with fibrocystic change and one with granulomatous mastitis.
Abbreviations: DCIS, ductal carcinoma in situ; IDC, invasive ductal carcinoma; ILC, invasive lobular carcinoma.

**Table 3.** Qualitative Data on Mass Location, According to the Fibroglandular Interface (FGI) and Anatomic Quadrants by Mass Type. The All Benign Group (*N* = 220) was Composed of the Sum of the Fibroadenoma (*N* = 105), Cyst (*N* = 91), and Other Benign (*N* = 24) Categories

| | FGI Tissue Locations *n*/*N* (%) | | | Anatomic Quadrants *n*/*N* (%) | | | |
|---|---|---|---|---|---|---|---|
| **Mass type** | **At FGI** | **In Fibro-glandular** | **In Fat** | **Upper Outer** | **Upper Inner** | **Lower Outer** | **Lower Inner** |
| Cancer[a] | 74/78 (95) | 0/78 (0) | 4/78 (5) | 34/78 (44) | 17/78 (22) | 17/78 (22) | 10/78 (13) |
| All Benign[b] | 120/220 (55) | 98/220 (45) | 2/220 (1) | 85/220 (39) | 46/220 (21) | 64/220 (29) | 25/220 (11) |
| Fibroadenoma[a] | 66/105 (63) | 37/105 (35) | 2/105 (2) | 39/105 (37) | 25/105 (4) | 29/105 (28) | 12/105 (11) |
| Cyst[a] | 33/91 (36) | 58/91 (64) | 0/91 (0) | 39/91 (43) | 15/91 (16) | 29/91 (32) | 8/91 (9) |
| Other Benign[a] | 21/24 (88) | 3/24 (13) | 0/24 (0) | 7/24 (29) | 6/24 (25) | 6/24 (25) | 5/24 (21) |
| Totals | 194/298 (65) | 98/298 (33) | 6/298 (2) | 119/298 (40) | 63/298 (21) | 81/298 (27) | 35/298 (12) |

[a]Overall *P* value for FGI tissue locations between mass types (cancer, fibroadenoma, cysts, other benign), *P* < 0.00.
[b]Overall *P* value between cancer and all benign, *P* < 0.001. Similarly, overall *P* values for mass types and cancer versus all benign for anatomic quadrants were *P* = 0.648 and *P* = 0.658.
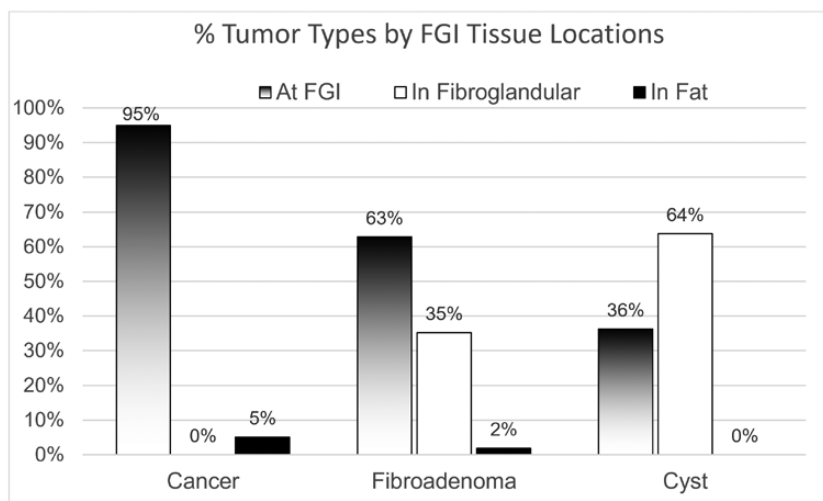
**Figure 4.** Fibroglandular interface (FGI) tissue locations for each tumor type from Table 3. Note: The "other benign" category was not shown for clarity due to their small numbers.

**Table 4.** Quantitative Tumoral and Peritumoral Results for All Masses

| Mass type | Mean Tumor SS (m/s) | Mean Peritumor SS (m/s) | Tumor to Peritumor SS Difference (m/s) | Tumor to Peritumor SS Ratio | Mean Tumor PFG (%) | Mean Peritumor PFG (%) |
|---|---|---|---|---|---|---|
| Cancer | 1526.8 | 1476.7 | 50.1 | 1.034 | 83.5 | 47.1 |
| All Benign | 1534.1 | 1503.8 | 30.2 | 1.020 | 92.1 | 71.7 |
| *P*-value | 0.031 | <0.001 | <0.001 | <0.001 | <0.001 | <0.001 |
| Fibroadenoma | 1534.5 | 1495.8 | 38.6 | 1.026 | 92.5 | 65.3 |
| Cyst | 1535.5 | 1517.7 | 17.8 | 1.012 | 94.3 | 84.0 |
| Other Benign | 1526.7 | 1486.3 | 40.4 | 1.027 | 81.7 | 53.2 |
| *P*-value | 0.073 | <0.001 | <0.001 | <0.001 | <0.001 | <0.001 |

Abbreviations: PFG, percent fibroglandular tissue; SS, sound speed.

showed no significant mass differentiation. These qualitative appearances were supported by peritumoral analyses that segmented quantitative sound speed values and confirmed greater fat surrounding cancers and fibroglandular tissue surrounding most cysts.

Clinical mass location results were consistent with mammographic descriptions of greater occurrence of solid benign masses and cancers in the upper outer quadrants (1–3), making quadrant location alone insignificant for mass differentiation. The highly significant 95% cancer occurrence at the FGI by UST was similar to prior MRI studies (5,6) but now includes cysts and supportive quantitative tumoral:peritumoral data. Tumor location respective to the FGI is not a part of the US Breast Imaging Reporting and Database System (BI-RADS) (33), but as a potential future UST criterion, FGI location could be viewed as having a PPV of ~38%, or comparable to US BI-RAD Category 4B (ie, >10% to ≤50% likelihood of malignancy). These initial findings only used SS imaging for quantitation and further UST analytics suggest feasibility for future biological correlates, risk evaluation, and computer-aided detection and/or diagnostic efforts.

Cancer location at the FGI appears to be a reasonable visual search criterion for future UST screening of women with dense breasts. The circumferential periphery of the FGI is readily evaluated by the native coronal imaging plane of UST. Mass margins, as seen by UST, were visually compared to standard imaging and then hand-traced, which is clinically impractical. UST software using automated mass margin detection is being evaluated as part of computer-aided diagnostic efforts for further mass characterization. Moreover, future pixel-based enhancement of the fibroglandular margins that abut fat at the FGI, or associated fat-subtraction techniques, appear feasible and may improve cancer detection in women with dense breasts.

Our effort to quantify the FGI using tumoral:peritumoral data builds on UST work correlating SS imaging to mammographic density (15–18,20–22) and parenchymal distribution by MRI (19). The quantitative nature of SS imaging by UST implies that the peritumoral values are a better differentiator of mass type than values inside the tumor. Tumor ROI characterization by mean SS and percent fibroglandular tissue produced the weakest statistical
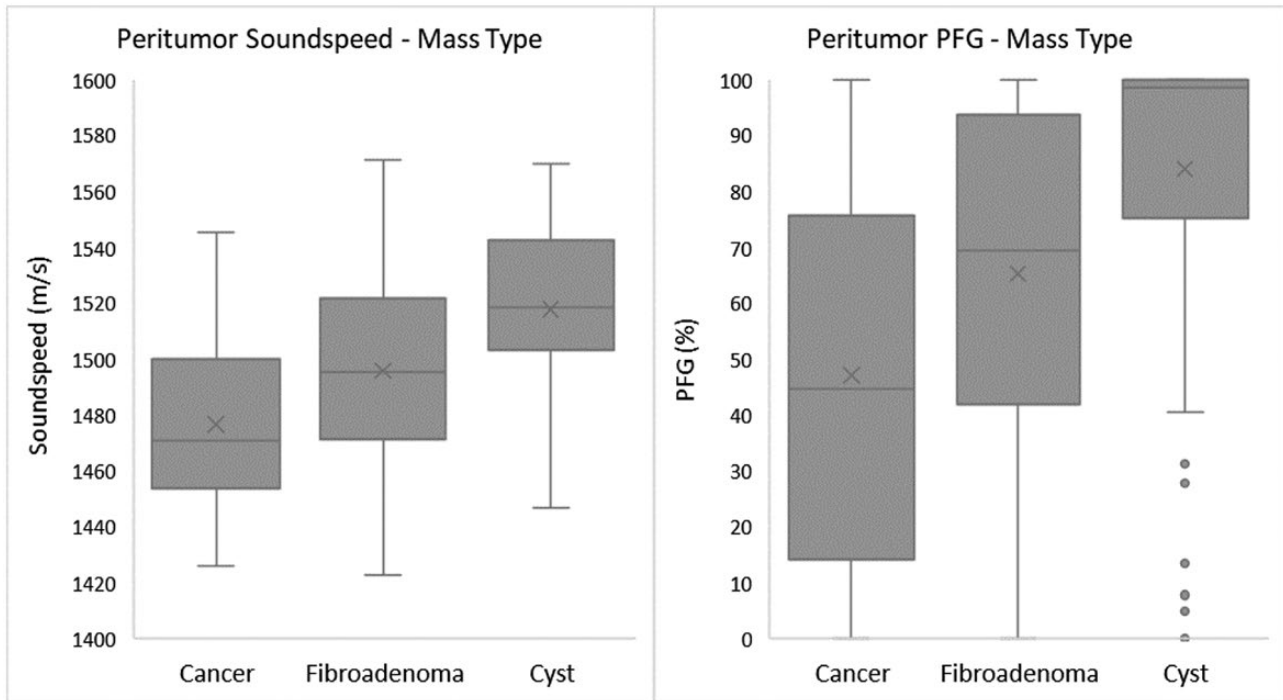
**Figure 5.** Boxplots of the quantitative mean peritumoral sound speed (left) and percent fibroglandular tissue (PFG) (right) grouped by mass type showing the highly significant peritumoral differences noted in Table 3. Note: The "other benign" category was not included due to their lower numbers.

characterizations ($P = 0.073$ and $P < 0.001$, respectively). The strength of the characterizations dramatically increased when the peritumoral regions were measured or compared to the tumoral regions. SS imaging is one of several different images created during a UST scan, and these other quantitative image stacks may contribute to tissue/tumor characterizations but were beyond the scope of this article concentrating on the FGI.

For mass evaluations, it may appear counterintuitive that the mean tumor SS of a cyst in this series (1536 m/s) displayed higher values than solid invasive cancers (1527 m/s). Some fibroadenomas may also have had fibrotic components to account for their high mean tumor SS (1535 m/s), which typically occurs as they involute after menopause. The cancers in this data set tended to be irregular in shape and/or have spiculated margins, making their true borders difficult to accurately trace. Cancer ROIs therefore may have inadvertently included some adjacent fat, such that ill-defined margins led to volume averaging and reduced mean tumor SS. Since cysts and fibroadenomas were more circumscribed, their traced boundaries would have more closely resembled their actual boundaries and limited this effect. Additionally, in breasts with multiple cysts, only 2 ROIs were drawn per breast and cysts, with a size of ~1 cm favored. Therefore, smaller cysts may have had cellular, proteinaceous, or inspissated debris that produced higher mean SS values (34,35), rather than common larger simple cysts with average mean SS approaching the value of water (eg, ~1520 m/sec).

Quantitative and volumetric SS parameters also have biological and clinical implications that warrant further work. From a whole breast perspective, defining the predominant origin of cancer at the FGI may better explain that only 20% of cancers occurred in the quadrant with the greatest percent density by MRI volumes (4). Cancer risk may relate more to the actual proportion of the FGI within each quadrant, such that the fat-related biological effects of cancer initiation (24–28) at the FGI may arise from random genetics occurring within susceptible adjacent fibroglandular tissue within any quadrant. While quantitative tumoral:peritumoral analyses confirmed that cancers were more likely to be surrounded by fat, further comparison of other UST parameters (ie, attenuation and stiffness) to pathology outcomes are needed to better understand biological changes within that fat. These may correspond to peritumoral MRI ADC values (29,30) and/or the stiff rim sign of elastography (31,32), suggesting the need for further developments of computer-aided diagnosis and detection, as well as the defining the optimum diameter and extent of the peritumoral band itself (29,30). Additional quantitative UST metrics may then be feasible for future computer-aided detection and mass characterization in support of dense breast screening and biological correlations. Finally, future quantitative comparisons to tissue specimens may offer insights to the complex biology of adipocytes, adipokines, and cancer cells near the FGI.

Several weaknesses are inherent when a single radiologist used a new breast imaging modality to analyze a subjective

criterion, such as the location of a breast tumor residing at the FGI. We chose a simplified three-point system (5,6) incorporating the extremes of a mass being completely surrounded by fat or fibroglandular tissue, compared to any combination of fat and fibroglandular tissue abutting a mass at the FGI. Yet the quantitative peritumoral analyses supported the subjective appearances of the FGI. Additional correlates of peritumoral UST analyses with biological and/ or molecular parameters are also needed, including larger analyses of different cancer types, as well as the peritumoral stiffness more often seen around hormone receptor positive cancers. While the UST coronal plane likely highlights tumor growth and detection (10,11), we also acknowledge that further work is needed on the three-dimensional assessment of both anterior and posterior tumor margins near the FGI. While no apparent recruitment bias was intended (ie, all breast densities eligible), no women with fatty breasts and only a few with scattered fibroglandular densities were encountered in this smaller clinical cohort from a much larger dense breast screening study. As such, our results may not be generalizable to women with lower breast density. Finally, this clinical data set may have been biased by including cancers and masses that were simply more likely to be seen, as opposed to those that may be found during screening from a future data set.

## Conclusions

The large majority of clinical breast cancers were visibly found by UST at the FGI, which is biologically relevant to cancer initiation and progression. The significantly greater occurrence of cancers at the FGI, compared to benign masses, was not true of anatomic quadrants where intra-quadrant frequency differences between the different types of masses were not significant. Moreover, quantitative UST results for individual masses and peritumoral regions corroborated the more subjective clinical appearance of greater fat surrounding cancers than benign masses. This study supports the use of the FGI to help guide future visual searches for clinical cancers, comparisons with their biological correlates, computer-aided detection and/or diagnostic efforts, and eventual incorporation into clinical practice for dense breast screening by UST.

## Conflict of Interest Statement

The following authors have a small amount of equity (<1%) in Delphinus Medical Technologies, Inc. (DMT) as either co-founders, employees, or board members.
Peter J. Littrup, MD; cofounder and Medical Advisor to the Chief Executive Officer of DMT.
Nebojsa Duric, PhD; Chief Technology Officer of DMT.
Mark Sak, PhD; Medical Imaging Physicist of DMT.
Cuiping Li, PhD; Director of Research of DMT.
Olivier Roy, PhD; VP of Engineering of DMT.
Rachel F. Brem, MD FACR FSBI; Board Member of DMT.
No disclosures noted for Mary Yamashita, MD; Principle Investigator.

## References

1. Perkins CI, Hotes J, Kohler BA, Howe HL. Association between breast cancer laterality and tumor location, United States, 1994-1998. *Cancer Causes Control* 2004;15(7):637–645.

2. Lee AH. Why is carcinoma of the breast more frequent in the upper outer quadrant? A case series based on needle core biopsy diagnoses. *Breast* 2005;14(2):151–152.

3. Venkatesan A, Chu P, Kerlikowske K, Sickles EA, Smith-Bindman R. Positive predictive value of specific mammographic findings according to reader and patient variables. *Radiology* 2009;250(3):648–657.

4. Chen JH, Liao F, Zhang Y, et al. 3D MRI for quantitative analysis of quadrant percent breast density: correlation with quadrant location of breast cancer. *Acad Radiol* 2017;24(7):811–817.

5. Kim WH, Li M, Han W, Ryu HS, Moon WK. The spatial relationship of malignant and benign breast lesions with respect to the fat-gland interface on magnetic resonance imaging. *Sci Rep* 2016;6:39085.

6. Zhu W, Harvey S, Macura KJ, Euhus DM, Artemov D. Invasive breast cancer preferably and predominantly occurs at the interface between fibroglandular and adipose tissue. *Clin Breast Cancer* 2017;17(1):e11–e18.

7. Rella R, Belli P, Giuliani M, et al. Automated breast ultrasonography (ABUS) in the screening and diagnostic setting: indications and practical use. *Acad Radiol* 2018;25(11):1457–1470.

8. Choi EJ, Choi H, Park EH, Song JS, Youk JH. Evaluation of an automated breast volume scanner according to the fifth edition of BI-RADS for breast ultrasound compared with hand-held ultrasound. *Eur J Radiol* 2018;99:138–145.

9. Chen JH, Lee YW, Chan SW, Yeh DC, Chang RF. Breast density analysis with automated whole-breast ultrasound: comparison with 3-D magnetic resonance imaging. *Ultrasound Med Biol* 2016;42(5):1211–1220.

10. Chae EY, Cha JH, Kim HH, Shin HJ. Comparison of lesion detection in the transverse and coronal views on automated breast sonography. *J Ultrasound Med* 2015;34(1):125–135.

11. Van Zelst JC, Platel B, Karssemeijer N, Mann RM. Multiplanar reconstructions of 3D automated breast ultrasound improve lesion differentiation by radiologists. *Acad Radiol* 2015;22(12):1489–1496.

12. Lover GH. Computerized time-of-flight ultrasonic tomography for breast examination. *Ultrasound Med Biol* 1977;3:117–127.

13. Duric N, Littrup P, Poulo L, et al. Detection of breast cancer with ultrasound tomography: first results with the Computed Ultrasound Risk Evaluation (CURE) prototype. *Med Phys* 2007;34(2):773–785.

14. Ranger B, Littrup PJ, Duric N, et al. Breast ultrasound tomography versus MRI for clinical display of anatomy and tumor rendering: preliminary results. *AJR Am J Roentgenol* 2012;198(1):233–239.

15. Duric N, Boyd N, Littrup P, et al. Breast density measurements with ultrasound tomography: a comparison with film and digital mammography. *Med Phys* 2013;40(1):013501.

16. Duric N, Littrup P, Li C, et al. Whole breast tissue characterization with ultrasound tomography. In *Medical Imaging: Ultrasonic Imaging and Tomography 2015; 9419: 94190G*. Bellingham, WA: International Society for Optics and Photonics; 2015.

17. Sandhu GY, Li C, Roy O, Schmidt S, Duric N. Frequency domain ultrasound waveform tomography: breast imaging using a ring transducer. *Phys Med Biol* 2015;60(14):5381–5398.

18. Sak M, Duric N, Littrup P, et al. Using speed of sound imaging to characterize breast density. *Ultrasound Med Biol* 2017;43(1):91–103.

19. O'Flynn EAM, Fromageau J, Ledger AE, et al. Ultrasound tomography evaluation of breast density: a comparison with noncontrast magnetic resonance imaging. *Invest Radiol* 2017;52(6):343–348.

20. Wiskin J, Malik B, Natesan R, Lenox M. Quantitative assessment of breast density using transmission ultrasound tomography. *Med Phys* 2019;46(6):2610–2620.

21. Duric N, Sak M, Fan S, et al. Using whole breast ultrasound tomography to improve breast cancer risk assessment: a novel risk factor based on the quantitative tissue property of sound speed. *J Clin Med* 2020;9:E367.

22. Sak M, Littrup P, Brem R, Duric N. Whole breast sound speed measurement from US tomography correlates strongly with volumetric breast density from mammography. *J Breast Imag* 2020;2(5):443–451.

23. Duric N, Littrup P, Sak M, et al. A novel marker, based on ultrasound tomography, for monitoring early response to neoadjuvant chemotherapy. *J Breast Imag* 2020;2(6):569–576.

24. Yamaguchi J, Ohtani H, Nakamura K, Shimokawa I, Kanematsu T. Prognostic impact of marginal adipose tissue invasion in ductal carcinoma of the breast. *Am J Clin Pathol* 2008;130(3):382–388.

25. Wang YY, Attané C, Milhas D, et al. Mammary adipocytes stimulate breast cancer invasion through metabolic remodeling of tumor cells. *JCI Insight* 2017;2:e87489.

26. Mancuso P. The role of adipokines in chronic inflammation. *Immunotargets Ther* 2016;5:47–56.

27. Dirat B, Bochet L, Dabek M, et al. Cancer-associated adipocytes exhibit an activated phenotype and contribute to breast cancer invasion. *Cancer Res* 2011;71(7):2455–2465.

28. Bochet L, Lehuédé C, Dauvillier S, et al. Adipocyte-derived fibroblasts promote tumor progression and contribute to the desmoplastic reaction in breast cancer. *Cancer Res* 2013;73(18):5657–5668.

29. McLaughlin RL, Newitt DC, Wilmes LJ, et al. High resolution in vivo characterization of apparent diffusion coefficient at the tumor-stromal boundary of breast carcinomas: a pilot study to assess treatment response using proximity-dependent diffusion-weighted imaging. *J Magn Reson Imaging* 2014;39(5):1308–1313.

30. Kettunen T, Okuma H, Auvinen P, et al. Peritumoral ADC values in breast cancer: region of interest selection, associations with hyaluronan intensity, and prognostic significance. *Eur Radiol* 2020;30(1):38–46.

31. Zhou J, Zhan W, Chang C, et al. Breast lesions: evaluation with shear wave elastography, with special emphasis on the "stiff rim" sign. *Radiology* 2014;272(1):63–72.

32. Park HS, Shin HJ, Shin KC, et al. Comparison of peritumoral stromal tissue stiffness obtained by shear wave elastography between benign and malignant breast lesions. *Acta Radiol* 2018;59(10):1168–1175.

33. Mendelson EB, Böhm-Vélez M, Berg WA, et al. ACR BI-RADS® ultrasound. In: *ACR BI-RADS® Atlas, Breast Imaging Reporting and Data System*. Reston, VA: American College of Radiology; 2013.

34. Iuanow E, Smith K, Obuchowski NA, Bullen J, Klock JC. Accuracy of cyst versus solid diagnosis in the breast using quantitative transmission (QT) ultrasound. *Acad Radiol* 2017;24(9):1148–1153.

35. Malik BH, Klock JC. Breast cyst fluid analysis correlations with speed of sound using transmission ultrasound. *Acad Radiol* 2019;26(1):76–85.